Anisotropic Diffusion of Elongated and Aligned Polymer Chains In a Nematic Solvent†

Stephan Link,‡ Wei-Shun Chang,‡ Arun Yethiraj,*,§ and Paul F. Barbara*,‡

Department of Chemistry and Biochemistry and the Center for Nano- and Molecular Science and Technology, University of Texas at Austin, Austin, Texas 78712, and Department of Chemistry, University of Wisconsin, Madison, Wisconsin 53706

Received: March 28, 2006; In Final Form: May 22, 2006

The translational diffusion constant, D, of a polymer *solute* in a single-domain, nematic liquid crystal *solvent* (5CB) is measured in directions parallel and perpendicular to the nematic director using a fluorescence two-beam, cross-correlation technique. The solute under investigation is the stiff, conjugated polymer, MEH-PPV. The ratio $D_{||}/D_{\perp}$ of diffusion constants (parallel and perpendicular to the director) is observed to be 1.9 $\pm$ 0.3. This is surprisingly small considering that MEH-PPV is known to be both elongated and highly aligned along the liquid crystal director of 5CB. We therefore argue that the structural order parameter of the solvent governs the anisotropy of the diffusion of the solute.

Introduction

The anisotropic translational diffusion of molecules in anisotropic environments is of growing experimental and theoretical interest.[1−7] A particularly well-defined model system is a single-domain, thermotropic nematic liquid crystal (LC), containing a dilute "probe" solute.[2,8−10] Diffusion anisotropy in this cylindrically symmetric system is quantified by the ratio of probe diffusion constant parallel and perpendicular to the nematic director, that is, $D_{||}/D_{\perp}$. Various theoretical models[7,11−14] have been developed for $D_{||}/D_{\perp}$ as a function of the order parameter S in the nematic LC phase. Because the viscosity of the nematic solvent is itself anisotropic, the diffusion of even spherical solutes is moderately anisotropic, for example, $D_{||}/D_{\perp} \approx 1.6$ for spheres in a nematic liquid crystal.[1] Experimental results on the diffusion anisotropy of solutes in common thermotropic nematic LCs reveal a broad range of $D_{||}/D_{\perp}$ values.[2,8−10] For fluorescence probe solutes with sizes comparable to those of the LC solvent molecules, $D_{||}/D_{\perp}$ values ranging from ~1.1−4 have been observed, using fluorescence correlation spectroscopy,[2] forced Rayleigh scattering,[8−10] and fluorescence photobleaching recovery spectroscopy.[15]

Theory predicts even larger $D_{||}/D_{\perp}$ values[12−14] for the *self-diffusion* of highly ordered (macro-)molecules with large aspect ratios due, qualitatively, to the combined effect of the anisotropy of the translational friction of such rodlike molecules and the tendency for rodlike molecules to be highly aligned in the nematic LC phase. This was just recently confirmed for the self-diffusion of the colloidal rodlike virus *fd*, which has an aspect ratio greater than 100 and forms a lyotropic LC at high concentrations.[16] By video imaging of individual dye-labeled *fd* virus molecules dissolved in a background of nonlabeled viruses, diffusion anisotropies $D_{||}/D_{\perp}$ ranging from 7.5 to >20 were determined in the nematic phase as a function of increasing order parameter. Our work addresses the following question: What is the diffusion anisotropy of a highly aligned and elongated probe dissolved in the nematic phase of a low molecular weight LC solvent?

In this work, the directional diffusion constant of a fluorescent probe molecule is determined from the intensity cross-correlation of fluorescence originating from the same molecule diffusing through two spatially separated probe volumes. A new chopping/synchronous-detection scheme is employed to reject a serious cross-talk background in the data. The probe molecule used in this study is the rodlike conjugated polymer MEH-PPV, and the solvent is the thermotropic LC 5CB. We have shown recently that MEH-PPV molecules are highly aligned in 5CB, with an order parameter, $S = {}^1/_2\langle 3\cos^2\alpha - 1\rangle$, of 0.99 compared to 0.48 for 5CB,[17] where α is the angle between the long axis of the MEH-PPV molecule and the LC director.[18,19] In addition, recent results have shown that the conformation of MEH-PPV is elongated along the director.[19] With information on the shape of the probe molecules, we are able in this work to make predictions for $D_{||}/D_{\perp}$ and compare the predicted values to the experimental value obtaining new insight into the anisotropy of molecular diffusion in an anisotropic environment. Our main conclusion is that the translational dynamics of the solute is governed primarily by the nematic order of the solvent.

Sample Preparation Method

Single domain LC films of MEH-PPV-doped 5CB (Aldrich) with a concentration of 10^{-6}−10^{-8} % by weight are prepared starting from a polymer−5CB−chlorobenzene triphase system.[20] After evaporation of the chlorobenzene, the MEH-PPV-5CB mixtures are sandwiched between PVA-coated quartz slides and glass coverslips separated by a 50 μm Mylar spacer. The alignment of the LC films is verified by optical polarization microscopy (Zeiss Axioskop 2 MAT). The MEH-PPV sample employed in this study has a mean molecular weight of 110 000, corresponding to 423 repeat units per chain. The sample has a single bond defect concentration of 2%, which forces bends in the polymer chains separated by about every 50 repeat units.[19]

Two-Beam Fluorescence Cross-Correlation Apparatus

The fluorescence cross-correlation experiments are performed on a home-built confocal microscope (Figure 1) with two

† Part of the special issue "Charles B. Harris Festschrift".

* Corresponding authors: E-mail: p.barbara@mail.utexas.edu; yethiraj@chem.wisc.edu.

‡ University of Texas at Austin.

§ University of Wisconsin.

10.1021/jp061929u CCC: $33.50
Published on Web 06/30/2006

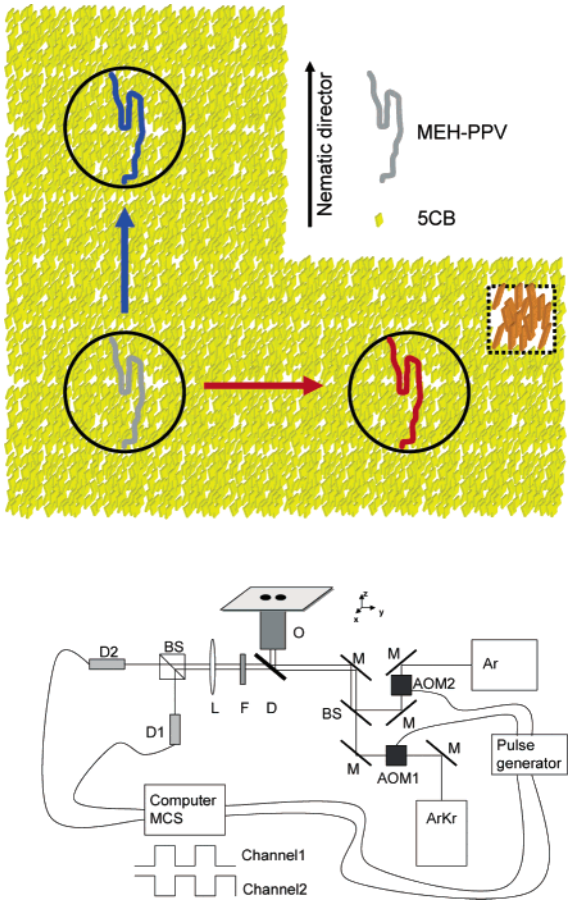

Figure 1. Schematic illustration (top) and experimental realization (bottom) of the two-beam cross-correlation setup. M, mirror; AOM, acousto-optic modulator; BS, 50/50 beam splitter; D, dichroic; O, objective; F, filter; L, lens; D, detector; MCS, multichannel scaler.

independent focal volumes/detector system channels. The apparatus is based on an inverted microscope (Zeiss Axiovert 200). Two laser beams are focused by the same objective (Zeiss Fluar, 100X, N.A. = 1.3) forming two independent diffraction-limited focal volumes in the nematic LC sample, a few micrometers above the coverslip. Independent continuous-wave ion laser sources are employed for the two respective focal volumes to remove spurious cross-correlation signals due to laser intensity fluctuations. The in-focal-plane separation distance of the focal volumes is variable in the range of 0−5 μm with a precision of 0.2 μm. The fluorescence from each laser focal volume is collected by the same objective, filtered by a dichroic and a band-pass filter, and independently imaged onto two separate detectors (APD, Perkin-Elmer SPCM). The 50/50 beam splitter between the body of the microscope and the detectors is used simply for alignment convenience, and both replicas from the beam splitter each produce two focal spots, but only one is focused on its respective detector. Confocal "spatial filtering" conditions for collection of the fluorescence light originating from each of the two laser spots is achieved by using a total image magnification of 850X at the APD detectors (which have an active area of 175 μm). Confocal conditions for detection are necessary in this experiment to narrow the spatial resolution for the diffusion measurements. The LC samples are mounted on a rotation stage allowing for convenient alignment of the director with respect to the direction of the displacement of the two focal volumes.

To remove fluorescence intensity cross-talk between the focal volumes, that is, detection of fluorescence from the "wrong" focal volume, the two excitation beams are chopped with opposite phase, using two acousto-optic modulators (IntraAction Corp. AOM 403R). The APD outputs are synchronously gated at the input of the counter board (Becker&Hickl PMS-400). The modulation frequency is chosen to be 100 times larger than the bin time (10 ms). Thus, the setup is functionally equivalent to two independent confocal microscopes where each one monitors a different region of the sample separated by only a few micrometers (Figure 1).

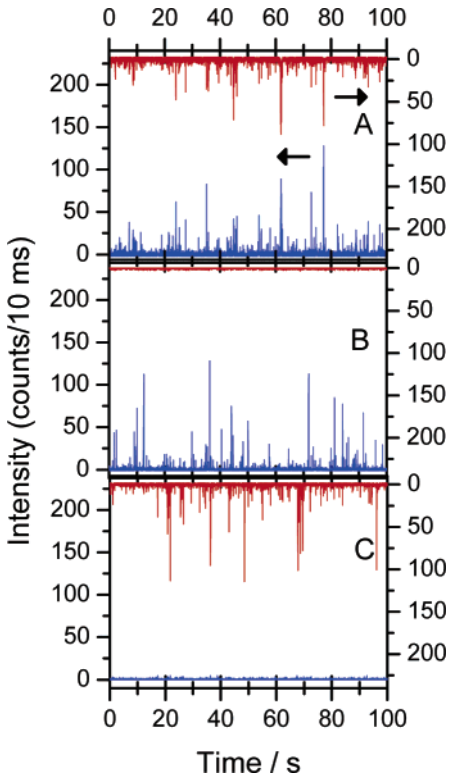

Figure 2. Dual-channel fluorescence transients from MEH-PPV in 5CB for a beam separation of 0 μm. Part A shows the raw signal with both beams on, and parts B and C were recorded with either laser beam blocked. This illustrates complete suppression of cross-talk originating from the opposite probe volume even at 0 μm beam separation.

Results and Discussion

The chopping scheme described above is crucial for eliminating background and makes the cross-correlation measurement feasible. Figure 2A shows dual-channel fluorescence intensity transients from MEH-PPV in 5CB with overlapping focal volumes, that is, $r = 0$ μm. The individual blips correspond to single molecules passing through the two focal volumes, which in this case are overlapped. The intensity for the two channels is plotted in opposite vertical directions in the plot in order to make the individual transients easier to visualize. The analogous transients recorded with either one or the other laser beams blocked are shown in Figure 2B and C, respectively. These data demonstrate that the chopping/synchronous detection scheme (described above) completely suppresses the cross-talk originating from the opposite probe volume, even at $r = 0$ μm focal volume separation. Without the chopping/synchronous detection scheme, cross-talk due to overlapping focal volumes (which includes diffraction rings) is a large background, and a major complication for the cross-correlation measurement. Our setup is therefore a significant improvement over a previously described two-beam cross-correlation technique that did not employ chopping.[21]

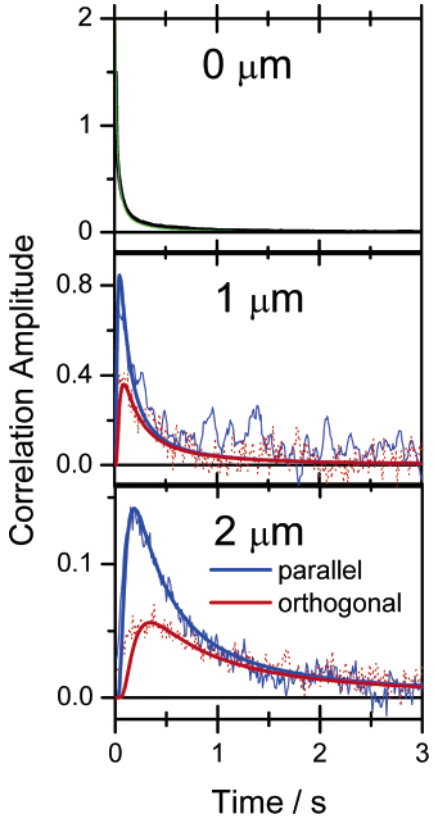

Figure 3. Autocorrelation (top, 0 μm) and two-beam cross-correlations at beam separations of 1 μm (middle) and 2 μm (bottom) for MEH-PPV diffusing in 5CB. For both beam separations, the cross-correlations were fitted (solid lines) according to eq 2 with diffusion constants of $D_{\|} = (3.8 \pm 0.5) \times 10^{-12}$ m^2 s^{-1} and $D_{\perp} = (2.0 \pm 0.5) \times 10^{-12}$ m^{2}s^{-1} for parallel (blue) and perpendicular (red) diffusion with respect to the LC director. The autocorrelation was calculated using the isotropic average, i.e., $\langle D \rangle = (D_{\|} + 2D_{\perp})/3 = (2.6 \pm 0.5) \times 10^{-12}$ m^2 s^{-1}.

Diffusion constants are obtained by fitting the fluorescence cross-correlation $G_c(\tau)$, obtained from the intensity transients, $F(t)$, to a model. $F(t)$ is acquired with a bin time of 10 ms. We acquire data for periods up to several hours, which is necessary to achieve an adequate signal-to-noise, especially for the large beam separations, because the cross-correlation amplitude decays rapidly with distance. The fluorescence cross-correlation $G_c(\tau)$ is obtained from the analysis of $F(t)$, as follows:[22]

$$G_c(\tau) = \frac{\langle \delta F_1(t) \cdot \delta F_2(t+\tau) \rangle}{\langle F_1(t) \rangle \cdot \langle F_2(t) \rangle} \quad (1)$$

Here τ is the lag time, $F_1(t)$ and $F_2(t)$ are the fluorescence intensities measured by the two detectors, and the brackets denote time-averaged values.

To increase the signal-to-noise ratio of the $G_c(\tau)$, intensity bursts in $F(t)$ are first subjected to a threshold condition allowing us to remove unwanted signal from smaller MEH-PPV molecules and background counts from 5CB. The experimental results for MEH-PPV diffusing in 5CB are shown in Figure 3 for beam separations corresponding to 0 μm (essentially an autocorrelation, top), 1 μm (middle), and 2 μm (bottom). The lines through the data are fits for the focal volume separation axis parallel (blue) and perpendicular (red) to the LC director. The $G_c(\tau)$ at a beam separation of 2 μm shows a pronounced anticoincidence at early times consistent with the fact that the same molecule cannot be present in both detection volumes at the same time.

The $G_c(\tau)$ data are analyzed employing an analytical model that is closely analogous to previous reports.[21−23] The model is based on the assumptions that the fluorescence intensity fluctuation is due only to concentration fluctuations of the MEH-PPV, the focal spots have a 3D Gaussian beam profile, and the concentration of MEH-PPV follows a Poisson distribution. This leads to the following expression of $G_c(\tau)$ for molecules diffusing between the two detection volumes

$$G_c^{x,y}(\tau) = \frac{1}{\langle C \rangle \pi \sqrt{4D_x\tau + w_0^2}\sqrt{4D_y\tau + w_0^2}\sqrt{4D_z\tau + z_0^2}} e^{-r^2/4D_{x,y}\tau + w_0^2} \quad (2)$$

where $\langle C \rangle$ is the mean concentration of MEH-PPV, w_0 is the $1/e^2$ radius of the Gaussian beam in the sample plane (xy), $2z_o$ is the height of the focal volume, and r is the distance between the two laser spots. $G_c^x(\tau)$ and $G_c^y(\tau)$ correspond to diffusion parallel and perpendicular to the LC director. Values of $w_0 =$ 100 nm and $z_0/w_0 = 5$ were used in the analysis.

The solid lines in Figure 3 are best fits of the data using eq 2, and agree well with the experimental results. The fit procedure involved first fitting the autocorrelation data (Figure 3A) using an isotropic diffusion constant, that is, $\langle D \rangle = (D_{\|} + 2D_{\perp})/3$, and then using $\langle D \rangle$ as a constraint for the data with beam separations of 1 and 2 μm. However, a three-parameter global fit gives similar results. From the best-fit parameters, we obtained $D_x = D_{\|} = (3.8 \pm 0.5) \times 10^{-12}$ m^2 s^{-1} and $D_z = D_y = D_{\perp} = (2.0 \pm 0.5) \times 10^{-12}$ m^{2}s^{-1}. The excellent agreement between experiment and predicted curves supports the validity of the overall method of analysis. Finally, using the best-fit values a diffusion anisotropy ratio $D_{\|}/D_{\perp} = 1.9 \pm 0.3$ can be determined for MEH-PPV in 5CB.

There are two sources of diffusion anisotropy for solutes in liquid crystalline solvents. The first is the anisotropy of the solute itself, and the second is the anisotropy in the friction between the solute and the solvent. Consider, for example, the dynamics of a rodlike molecule. Physically, one expects its diffusion in the direction along its axis to be less hindered than that in the direction perpendicular to its axis. In a dilute solute of rods in an isotropic solvent, for example, one has $D_{\|}/D_{\perp} = 2$.[24] The anisotropy of the friction with the solvent can also induce an anisotropic diffusion because the solvent friction is lower along the nematic director, and for a sphere in a nematic solvent, $D_{\|}/D_{\perp} \approx 1.6$.[1,6] One might therefore expect $D_{\|}/D_{\perp} > 2$ for rods in a nematic solvent.

Most theories have addressed the self-diffusion of anisotropic molecules in the nematic phase. For very long rods in semidilute *isotropic* solutions, $D_{\perp} \approx 0$ and the diffusion anisotropy is infinite. For the self-diffusion in the nematic phase, a number of models have been proposed. Models by Hess, Frenkel, and Allen (HFA)[14] and by Chu and Moroi (CM)[13] for the self-diffusion of nematic LCs predict that the molecular diffusion anisotropy strongly increases with increasing order parameter S and aspect ratio e. In these models, the diffusion anisotropy becomes *independent* of e for large e, and in the asymptotic limit of infinite e, $D_{\|}/D_{\perp} = (1 + 2S)/(1 - S) = 3.8$ for $S =$ 0.48. Computer simulations of hard spherocylinders[12] have confirmed this prediction as an upper bound to the anisotropy and also demonstrated that $D_{\|}/D_{\perp}$ is independent of e over the range ($4 \le e \le 16$) they studied. For $S = 0.48$, the simulations find that $D_{\|}/D_{\perp} \approx 2-2.5$, independent of e. A diffusion anisotropy of 1.9 ± 0.3 is surprisingly small in light of the high

TABLE 1: Comparison of Experimental and Theoretical Results for the Anisotropy Ratio $D_{||}/D_{\perp}$ for MEH-PPV in 5CB[a]

model/reference [no.]	$D_{||}/D_{\perp}$	equations
experiment	1.9	
Hess, Frenkel, Allen (HFA) $S = 0.48$ (0.99), $e = 9.2$ [13]	3.6 (65.8)	$D_{||} = \langle D\rangle_g \kappa[e^{4/3} - 2e^{-2/3}(e^2 - 1)(1 - S)/3]$ $D_{||} = \langle D\rangle_g \kappa[e^{-2/3} - 2e^{-2/3}(e^2 - 1)(1 - S)/3]$
Chu and Moroi (CM) $S = 0.48$ (0.99), $e = 9.2$ [14]	3.1 (11.2)	$D_{||} = \langle D\rangle[1 + (2 - 2\pi/4e)/(1 + 2\pi/4e)S]$ $D_{\perp} = \langle D\rangle[1 - (1 - \pi/4e)/1 + 2\pi/4e)S]$
Kirkwood−Riseman (KR) $R_G = 30.0$ nm [27]	1.7	$D_{||} = 4kT/9\pi^2\eta_{||}R_G$ $D_{\perp} = 4kT/9\pi^2\eta_{||}R_G$
Garcia de la Torre (GT) cylinders/ellipsoids (stick boundary cond.), $L = 88.8$ nm, $e = 9.2$ [28−30]	2.4	$D_{||} = (kT/2\pi\eta_{||}L)(\ln e + \nu_{||})$ $D_{\perp} = (kT/4\pi\eta_{||}L)(\ln e + \nu_{\perp})$
Tang and Evans (TE)/Allison ellipsoids (slip boundary cond.), $L = 88.8$ nm, $e = 9.2$ [31,32]	9.2/6.9	calculated with numerical values for D_{slip}/D_{stick} according to TE/Allison

[a] The polymer dimensions were calculated from conformations obtained by Monte Carlo simulations of 100 beads representing 250 repeat units and having 15 defects in a LC solvation potential[19] and were scaled up to the molecular weight (MW) of the experimental sample according to $MW^{3/5}$. $\langle D\rangle_g = (D_{||}^{1/3} \cdot D_{\perp}^{2/3})$ is the geometric average for the isotropic diffusion constant. $\kappa = [1 + 2(e^{-2} - 1)(1 - S)/3]^{-1/3} \cdot [1 + (e^2 - 1)(1 - S)/3]^{-2/3}$. k = Boltzmann constant, T = temperature, R_G = radius of gyration. $\nu_{||}$ and $\nu_{\perp}$ are end-effect correction factors and are functions of the aspect ratio e. For all other definitions, refer to the text.

orientational anisotropy of the MEH-PPV chains and the fact that for the self-diffusion of 5CB $D_{||}/D_{\perp} = 2.7$.[25,26]

It is of interest to adapt the models for the self-diffusion of nematic LCs to the tracer diffusion of solutes in nematic solvents. The two parameters in the models are the aspect ratio of the molecules and the nematic order parameter. For MEH-PPV in 5CB, the solute order parameter is $S = 0.99$,[19] and using this value in the models gives diffusion anisotropies that are far too large, that is, 65.8 and 11.2, respectively, in the HFA and CM theories (see Table 1). We therefore conclude that the appropriate order parameter in the models is that of the solvent, and this gives diffusion anisotropies of 3.6 and 3.1, respectively, for the HFA and CM theories, for $S = 0.48$.[17] This is in much better agreement with experiment, although the models significantly overestimate the anisotropy measured in experiment.

Extensions of the hydrodynamic theory by Kirkwood and Riseman (KR)[27] to our system using the anisotropy of the solvent viscosity ($\eta_{||}/\eta_{\perp} = 1.7$)[6] give predictions in reasonable accord with our experiments. To account for the nonspherical shape of MEH-PPV, we compute the diffusion constants of a cylindrically shaped polymer with length L and aspect ratio e according to a hydrodynamic model by Garcia de la Torre (GT) and co-workers.[28−30] For cylinders, the *intrinsic molecular diffusion anisotropy* in dilute (isotropic) solutions increases slowly with increasing aspect ratio. In case of the modeled conformation of our MEH-PPV sample, the intrinsic diffusion anisotropy is 1.4 for an aspect ratio of 9.2. The experimentally observed diffusion anisotropy for a cylinder in a LC solvent is then the product of the intrinsic diffusion anisotropy and the anisotropy of the solvent viscosity yielding a diffusion anisotropy of 2.4, which is in reasonable agreement with our measurements. The predictions of various theories for the diffusion anisotropy are collected in Table 1, where the solute geometric parameters are obtained from a previously modeled[19] MEH-PPV conformation.

The experiments shed light on the hydrodynamic boundary conditions for solute diffusion in nematic solvents. The anistropic diffusion of rods is qualitatively different for stick and slip boundary conditions. In the case of stick, the friction scales with the length of the rod in both the parallel and perpendicular directions, and the diffusion anisotropy becomes independent of the aspect ratio in the limit of large e. In the case of slip, however, the friction in the direction parallel to the rod axis is independent of the aspect ratio and the anisotropy becomes an increasing function of the length of the rod. The small value of the diffusion anisotropy for $e = 9.2$ suggests that stick boundary conditions are more appropriate for polymers in a nematic solvent. This conclusion can be made more quantitative by comparing to numerical solutions for hard ellipsoids.[31,32] If we use our estimated aspect ratio and calculate the diffusion anisotropy based on slip boundary conditions using the numerical results of Tang and Evans (TE)[31] and Allison,[32] respectively, then we obtain values of $D_{||}/D_{\perp} = 9.2$ and 6.9, which is much larger than the anisotropy measured. We therefore conclude that stick is the more appropriate boundary condition for this system.

It is worthwhile to briefly discuss why the observed diffusion anisotropy for MEH-PPV is smaller than the values predicted by theory and also smaller compared to the anisotropy of perylene in a nematic LC mixture measured by a similar fluorescence correlation technique ($D_{||}/D_{\perp} = 4.0$),[2] as well the anisotropy for the solvent self-diffusion ($D_{||}/D_{\perp} = 2.7$).[25,26] In the calculations, we have neglected the effect of the polymer solute on the intrinsic solvent viscosity. An increase in the viscosity might have a larger effect on the diffusion parallel to the long polymer axis, thus reducing the observed diffusion anisotropy. This could be rationalized qualitatively in the following way. The friction for the parallel motion of the polymer is enhanced because of the segmented nature of the polymer chain. Because of defects along the polymer chain, our MEH-PPV sample typically consists of about 8−10 segments despite the rigid nature of the conjugated backbone. If the diffusion of an individual segment is similar to the solvent, then one would expect that for the linked segments in a stretched polymer chain the parallel diffusion is hindered because the segments tend to run into each other more frequently in the parallel direction. In addition, the large size of the polymer compared to the solvent makes the chain sample the solvent much more than shorter molecules, which has the effect of reducing the diffusion anisotropy to that of a sphere. Therefore, it should be emphasized that the presence of defects along the

polymer chain partially limits the ability to rigorously compare the different theoretical models.

Conclusions

The translational diffusion constant of a polymer *solute* in a single nematic LC (5CB) *solvent* is measured for directions parallel and perpendicular to the LC director (i.e., $D_{\|}$ and $D_{\perp}$, respectively) using a fluorescence two-beam, cross-correlation technique. The solute under investigation is the stiff, conjugated polymer, MEH-PPV. The diffusional anisotropy ratio $D_{\|}/D_{\perp}$ is observed to be 1.9 ± 0.3, which is surprisingly small since MEH-PPV is known to be both elongated and highly aligned along the LC director of 5CB due to cooperative solvation along the polymer chain. These results suggest that the diffusional anisotropy of macromolecules in anisotropic media is rather insensitive to the solute's alignment and conformation but is dominated mainly by the properties of the solvent.

Acknowledgment. This material is based upon work supported by the National Science Foundation under Grant No. CHE-0416112 to P.F.B. and Grant No. CHE-0315219 to A.Y. P.F.B. acknowledges support from the Keck Foundation and the Welch Foundation.

References and Notes

(1) Loudet, J. C.; Hanusse, P.; Poulin, P. *Science* **2004**, *306*, 1525.
(2) Kawai, T.; Yoshihara, S.; Iwata, Y.; Fukaminato, T.; Irie, M. *ChemPhysChem* **2004**, *5*, 1606.
(3) Yin, Y.; Zhao, C.; Kuroki, S.; Ando, I. *Macromolecules* **2002**, *35*, 2335.
(4) van Bruggen, M. P. B.; Lekkerkerker, H. N. W.; Maret, G.; Dhont, J. K. G. *Phys. Rev. E* **1998**, *58*, 7668.
(5) Krueger, G. J. *Phys. Rep.* **1982**, *82*, 229.
(6) Stark, H.; Venttzki, D. *Phys. Rev. E* **2001**, *64*, 31711.
(7) Darinsjii, A. A.; Zarembo, A.; Balabaev, N. K.; Neelov, I. M.; Sundholm, F. *Phys. Chem. Chem. Phys.* **2003**, *5*, 2410.
(8) Hara, M.; Ichikawa, S.; Takezoe, H.; Fukuda, A. *Jpn. J. Appl. Phys.* **1984**, *23*, 1420.
(9) Spiegel, D. R.; Thompson, A. L.; Campell, W. C. *J. Chem. Phys.* **2001**, *114*, 3842.
(10) Urbach, W.; Hevet, H.; Rondelez, F. *J. Chem. Phys.* **1985**, *83*, 1877.
(11) Vasanthi, R.; Ravichandran, S.; Bagachi, B. *J. Chem. Phys.* **2001**, *114*, 7989.
(12) Loewen, H. *Phys. Rev. E* **1999**, *59*, 1989.
(13) Chu, K.-S.; Moroi, D. S. *J. Phys. (Paris), Colloq.* **1975**, *36*, C1.
(14) Hess, S.; Frenkel, D.; Allen, M. P. *Mol. Phys.* **1991**, *74*, 765.
(15) Etchegoin, P. *Phys. Rev. E* **1999**, *59*, 1860.
(16) Lettinga, M. P.; Barry, E.; Dogic, Z. *Europhys. Lett.* **2005**, *71*, 692.
(17) Salamon, Z.; Skibinski, A. *Mol. Cryst. Liq. Cryst.* **1983**, *90*, 205.
(18) Lammi, R. K.; Fritz, K. P.; Scholes, G. D.; Barbara, P. F. *J. Phys. Chem. B* **2004**, *108*, 4593.
(19) Link, S.; Hu, D.; Chang, W.-S.; Scholes, G. D.; Barbara, P. F. *Nano Lett.* **2005**, *5*, 1757.
(20) Fritz, K. P.; Scholes, G. D. *J. Phys. Chem. B* **2003**, *107*, 10141.
(21) Brinkmeier, M.; Doerre, K.; Stephan, J.; Eigen, M. *Anal. Chem.* **1999**, *71*, 609.
(22) Schwille, P. *Cell Biochem. Biophys.* **2001**, *34*, 383.
(23) Elson, E. L.; Magde, D. *Biopolymers* **1974**, *13*, 1.
(24) Doi, M.; Edwards, S. F. *The Theory of Polymer Dynamics*; Clarendon Press: Oxford, 1986.
(25) Dvinskikh, S. V.; Furo, I. *J. Chem. Phys.* **2001**, *115*, 1946.
(26) Dvinskikh, S. V.; Furo, I.; Zimmermann, H.; Maliniak, A. *Phys. Rev. E* **2002**, *65*, 61701.
(27) Kirkwood, J. G.; Riseman, J. *J. Chem. Phys.* **1948**, *16*, 565.
(28) Tirado, M. M.; Garcia de la Torre, J. *J. Chem. Phys.* **1979**, *71*, 2581.
(29) Tirado, M. M.; Martinez, C. L.; Garcia de la Torre, J. *J. Chem. Phys.* **1984**, *81*, 2047.
(30) Ortega, A.; Garcia de la Torre, J. *J. Chem. Phys.* **2003**, *119*, 9914.
(31) Tang, S.; Evans, G. T. *Mol. Phys.* **1993**, *80*, 1443.
(32) Allison, S. A. *Macromolecules* **1999**, *32*, 5304.